



ORIGINAL ARTICLE

Thermal insulation performance of non-load-bearing light gauge slotted steel stud walls

Yuyin Wang^{a,b}, Faqi Liu^{a,b,*}, Hua Yang^{a,b}, Feng Fu^c, Yuteng Yan^{a,b}

^a Key Lab of Structures Dynamic Behavior and Control of the Ministry of Education, Harbin Institute of Technology, Harbin, 150090, China.

^b Key Lab of Smart Prevention and Mitigation of Civil Engineering Disasters of the Ministry of Industry and Information Technology, Harbin Institute of Technology, Harbin, 150090, China.

^c School of Engineering and Mathematical Sciences, City University, London, EC1V 0HB, U.K.

*Corresponding Author: Faqi Liu. Email: fqliu@hit.edu.cn.

Abstract: Light gauge steel stud walls have been widely used in buildings as load-bearing members. But if used as non-load-bearing walls, more rows of perforations can be placed on stud webs and then the thermal bridge effect can be reduced. Experiments on six non-load-bearing light gauge slotted steel stud walls were conducted using a calibrated hot box. The temperatures of the steel studs and gypsum plasterboard were monitored for subsequent analysis of thermal bridging. The effects of parameters (number of rows of perforations, stud web height, and the ratio of window area to wall area) on the insulating capacity of the wall were identified and analyzed. Thermal transmittance decreases by 18.5% and 29.6% for specimens with 3 and 7 rows of perforations in comparison with the specimen without perforations, while it decreases by 29.8% and 42.7% respectively for 150 mm and 200 mm thick walls compared with that of the 100 mm thick wall. However, thermal transmittance increases obviously for the wall with a window opening relative to the wall without a window opening, reaching 14.7% in this test since more studs are placed around the window opening. A three-dimensional finite element (FE) model of the wall was developed and validated against experimental results, and then was used for parametric studies. A general method of calculating the thermal transmittance of the light gauge slotted steel stud wall was suggested based on the experiment and the FE model results, which can consider influences of wall thickness, web perforations, window openings, and thermal properties of materials.

Keywords: Non-load-bearing light gauge slotted steel stud wall; thermal bridging effect; thermal insulation; design method; thermal transmittance

1 Introduction

The light gauge steel stud wall is fabricated using cold-formed steel studs, gypsum plasterboard, and insulating material [1] (**Fig. 1**) and has been widely used in buildings as a load-bearing member. It offers the benefits of rapid construction and energy saving. However, the cold-formed steel studs have much higher thermal conductivity than the interior insulation material, which creates thermal bridges and results in increased energy consumption, particularly in cold regions. Light gauge steel studs with slotted webs were proposed for external walls by researchers in Canada to reduce the effects of thermal bridging, which can greatly improve the thermal resistance of the wall. This kind of wall has been



certified as suitable for cold climates and has been widely used in Sweden, Finland, Canada, and the United States.

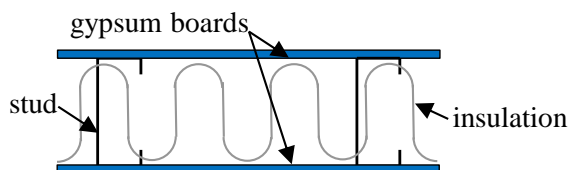


Fig. 1. Schematic view of the light gauge steel stud wall.

The light gauge steel stud wall has been extensively studied, and much is known about how it responds to axial compression [2-8], flexural [9-11], fire [12-24], and seismic activity [25-28]. For buildings in cold climates, the thickness of the wall may be determined by its thermal insulation properties. Höglund and Burstrand [29] calculated U-values (thermal transmittance) of light gauge slotted steel stud walls with different external insulation materials (brick façade, cavity insulation, and EPS board). Salonvaara and Nieminen [30] investigated the thermal performance of light gauge slotted steel stud walls by modelling, laboratory testing, and field measurement. They found that web perforations can reduce heat conduction along the web by 70%–80%. Elhajj [31] tested the thermal properties of light gauge slotted steel stud walls and calculated R-values (reciprocals of the U-values) for walls with solid or slit web studs and solid, slit, angle, or wood tracks. Lipták-Váradí [32] developed an equivalent thermal conductivity value for the slotted web of light gauge slotted steel stud walls. Moore et al. [33] determined the effect of thermal bridging on R-values for highly-insulated light gauge steel stud walls with vacuum insulation panels. Martins et al. [34] discussed several thermal bridge mitigation strategies and optimizations of wall insulation layers to improve the thermal performance of light gauge steel stud walls. Yang et al. [35] studied the influence of the slotted web on the thermal performance of a lightweight steel stud composite wall experimentally and numerically and recommended the dimensions of the slots (length, rows, transverse distance et) for practical applications.

Most previous studies recommended particular U-values or R-values for a light gauge slotted steel stud wall. However, these values are only applicable to a specific arrangement of studs. If the studs are arranged differently, the U-values and R-values would change obviously [29]. The ASHRAE modified zone method [35] can be used for calculating the thermal transmittance of steel stud walls. However, this method cannot consider the effect of the perforation on stud webs and thus is not applicable for the slotted steel stud wall in this paper.

If the light gauge steel stud wall with web perforations is used as a non-load-bearing wall instead of a load-bearing wall, more rows of perforations can be placed and the thermal insulation capacity can be improved. This non-load-bearing wall can be used in high-rise buildings, especially prefabricated structures because of its rapid construction. The subject of this study is the thermal insulation performance of non-load-bearing light gauge slotted steel stud walls. For walls with openings (e.g., windows opening), additional studs need to be arranged around the openings of the wall, which would reduce the thermal insulation performance of the wall. A concept of stud percentage was introduced, which is the ratio of the stud flange area to the wall area, to investigate the influence of window openings on the insulation performance. Experiments and numerical analysis were performed to investigate the thermal insulation performance of the non-load-bearing light gauge slotted steel stud walls. Parameters were studied to quantify their influences on the thermal insulation of the wall, including the number of rows of perforations, web height, stud percentage, and thermal conductivity coefficients of wall fabrication materials. A general method was recommended to calculate the thermal transmittance of the stud walls, which considers the number of rows of perforations, window openings, wall thickness, and the thermal properties of constituent wall materials.

2 Experimental study

2.1 Test specimens

Six light gauge slotted steel stud walls were prepared for the experiments. Each specimen was referred to by a triplet consisting of web height (mm), the number of rows of perforations and the

opening factor (ratio of window area to wall area). To illustrate, specimen 150-3-0.45 was a specimen with 150 mm web height, three rows of perforations and an opening factor of 0.45. Specimens were varied in web height (100, 150 or 200 mm), the number of rows of perforations (0, 3 or 7) and opening factor (0 or 0.45), as shown in Tab. 1. For specimens 150-7-0.45, 100-4-0.45 and 200-9-0.45, the rows of perforations were increased as the wall thickness to maintain a constant value of the ratio of the heat transfer path length to web height, which is named as heat transfer path coefficient hereafter. Due to the dimensional constraints of the hot box, the specimens were designed to be 2400 mm \times 2400 mm. For the light gauge steel stud wall, the stud spacing is generally between 400 mm and 600 mm [37]. The thermal bridging effect is more obvious when the stud spacing is smaller [38], which is also the main concern of this study. Thus the stud spacing of 400 mm was adopted in the test to observe the thermal bridging effect. However, in the follow-up finite element parametric studies, the spacing was 600 mm considering that the partition wall has low requirements for the load-bearing capacity. The layouts of the walls, with or without window openings, are shown in Fig. 2. The dimensions of the perforations were 70 mm \times 3 mm, with a vertical spacing of 20 mm and horizontal spacing of 9 mm, as shown in Fig. 3.

Table 1. Details of specimens

NO.	Specimen no.	Height of web H (mm)	Rows of perforations n	Opening factor (window-to-wall area ratio) α	Heat transfer path coefficient
1	150-0-0	150	0	0	1.00
2	150-3-0	150	3	0	1.93
3	150-7-0	150	7	0	2.78
4	100-4-0.45	100	4	0.45	2.75
5	150-7-0.45	150	7	0.45	2.78
6	200-9-0.45	200	9	0.45	2.75

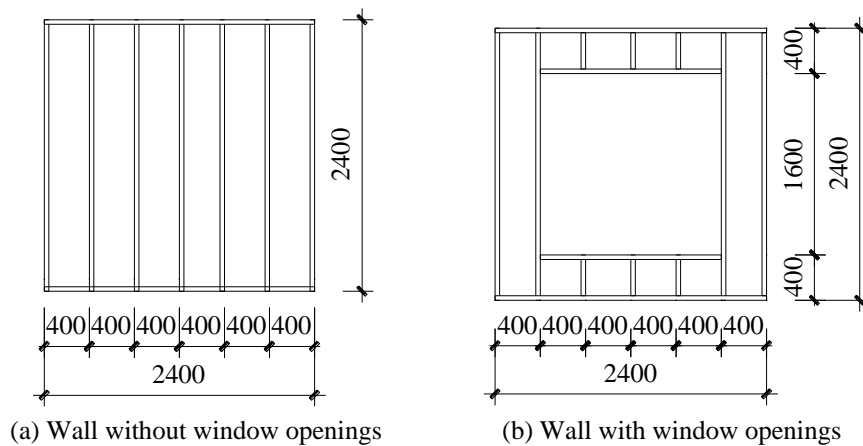


Fig. 2. Elevation of the wall (mm).

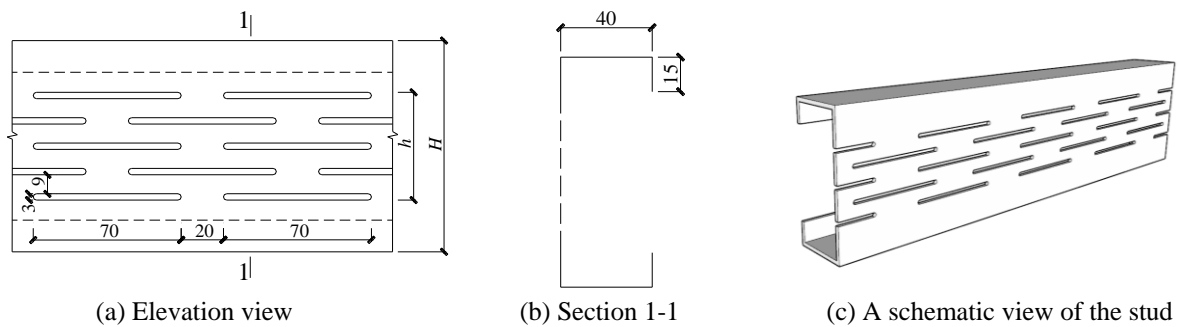


Fig. 3. The layout of slots on the web (mm).

The thickness of the gypsum board was 12 mm. Mineral wool with a density of 80 kg/m³ was used as wall interior insulation. The window opening was filled with extruded polystyrene (XPS) board with

the same thickness as the wall. Thermal conductivity and the area of the XPS board were measured before the experiments.

Groups of type T thermocouples were placed on the surface of the gypsum plasterboard for the identification of areas affected by thermal bridging (Fig. 4 (a) and (b)). Thermocouples were also mounted on the stud webs to measure temperatures at different wall locations for investigation of the effects of perforations on the thermal conductivity of the stud, as shown in Fig. 4 (c)-(e). Thermocouples in group X-1 were positioned to measure temperatures in a region affected by the thermal bridge. The distances between measurement points and the stud web were 0 mm, 50 mm, 100 mm, and 200 mm. Thermocouples in group X-2 were positioned close to the edge of the wall, where temperatures may be different from those detected in group X-1. Thermocouples in group X-3 measured temperatures at the stud joints to identify the influence of steel stud joints. Thermocouples in group X-4 measured the temperature distribution of the XPS board.

Thermal conductivities of the gypsum plasterboard, the mineral wool insulation, and the XPS were 0.21W/(m K), 0.037W/(m K) and 0.035W/(m K) respectively, which were measured following ISO 8302 [39], ISO 8990 [40] and Chinese code GB/T5480-2008 [41].

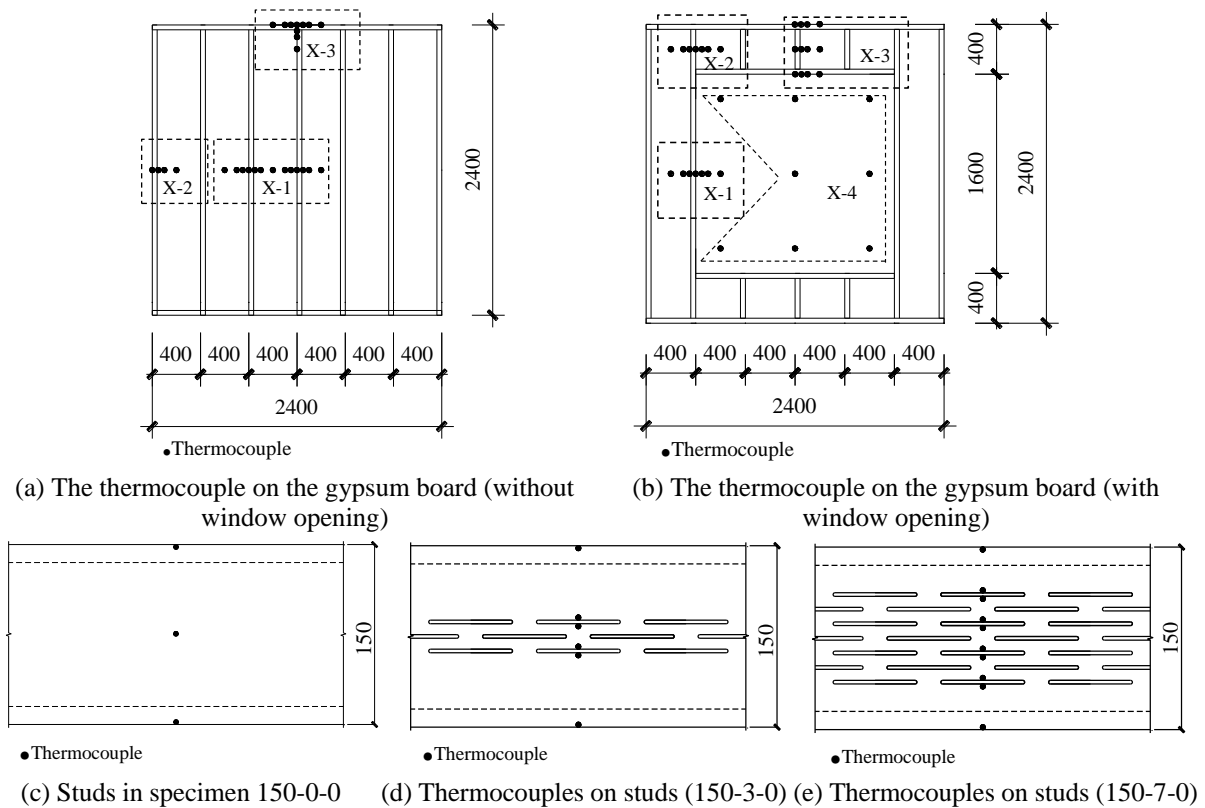


Fig. 4. Positions of thermocouple (mm).

2.2 Experimental setup

A statically calibrated hot box system was used to investigate the thermal insulation properties of the light gauge slotted steel stud walls in accordance with ISO 8990 [40], as shown in Fig. 5. The test equipment consists of a hot box, a cold box, a test track, air circulation and measurement systems and an automatic temperature control system. The maximum size of the specimen that could be tested was 2400 mm in length, 2400 mm in height and 400 mm in depth.

The hot box was designed on the assumption of steady-state heat transfer. The specimens were placed between the cold box and the hot box for the experiments. The cold box simulated outdoor winter weather conditions, and the hot box simulated indoor conditions. Measurements of the electrical power consumed by the hot box when the wall was in a state of steady heat transfer were used to calculate the heat transfer coefficient of each specimen.

The temperatures of the cold box and the hot box for all specimens were set as -10 °C and 18.0 °C,

respectively. The indoor temperature should be no lower than 18.0 °C for houses with heating systems in winter as suggested in Chinese code GB50176-2016 [42]. For different climatic regions, the minimum temperature in winter is different. Considering the condition of the test setup, the outdoor temperature was set to -10 °C. When the steady state was reached, the standard deviations of power, temperature and R-value (or U-value) were less than 1% within 3 hours. And when these values did not change monotonically, these experiments were stopped.



Fig. 5. A calibrated hot box system.

2.3 Experimental results

Fig. 6 shows the temperature distribution of specimens 150-0-0 (no perforations), 150-3-0 (three rows of perforations) and 150-7-0 (seven rows of perforations). It can be seen that the gradient of the temperature in the steel studs increases significantly as the number of rows of perforations increases (**Fig. 6** (a)), where y is the position of measurement points along with the wall thickness. The maximum temperature difference of the steel stud is 5.4 °C for specimens without perforations. When the number of rows of perforations increases to three or seven, the maximum temperature differences of steel studs are 12.9 °C and 18.2 °C respectively, as shown in **Fig. 6** (a). **Figs. 6** (b)- (e) show the temperatures of the hot (inside) and cold (outside) gypsum plasterboard surfaces, where x indicates the position of the measurement relative to the most left point ($x = 0$), and z indicates the position of the measurement relative to the most top point ($z = 0$). The surface temperature of the wall is non-uniform due to the thermal bridge effect of the steel studs. Take temperatures in group X-1 for example (**Fig. 6** (b)), the temperature of the cold surface close to the steel stud maximally increases by 4.55 °C, 2.13 °C and 1.77 °C relative to normal surface temperatures, respectively for the three specimens 150-0-0, 150-3-0 and 150-7-0. And the temperature of the hot surface of the wall decreases correspondingly by 1.19 °C, 1.15 °C and 0.91 °C respectively. These results indicate that the thermal bridge effect decreases significantly as the number of rows of perforations increases. Because the cold bridging of horizontal and vertical steel studs is superimposed at the stud joints, the thermal bridge effect at the joint is more obvious, as shown in **Fig. 6** (d) and (e). Take the temperatures in the vertical direction for example (**Fig. 6** (e)), the temperature of the hot surface near the stud joint maximally decreases by 2.31 °C, 2.93 °C and 1.19 °C relative to the temperature that far away from the joint ($z=0.2\text{m}$), respectively for the three specimens 150-0-0, 150-3-0 and 150-7-0. The specimen 150-0-0 should have worse performance than the specimen 150-3-0, however, the trend is odd in **Fig. 6** (d), which may be caused by test errors, deviations of thermocouple positions, etc.

Fig. 7 shows the temperatures for specimens 100-4-0.45, 150-7-0.45 and 200-9-0.45. As expected, the temperature of the hot side is higher and the temperature of the cold side is lower for the wall with a thickness of 200 mm compared with that of the wall with a thickness of 100 mm and 150 mm. The insulation of specimen 150-7-0.45 should be better than that of 100-4-0.45, but there is an odd trend in **Fig. 7**, which may be caused by test errors because temperature differences of these two specimens are

very small ($-0.18\text{ }^{\circ}\text{C} - 0.83\text{ }^{\circ}\text{C}$). The wall insulation performance can be enhanced by increasing the wall thickness, which can be concluded more obviously from the thermal transmittance (Tab. 2).

The typical comparisons between temperatures in groups X-1 and X-2 are presented in **Fig. 8** (a). Conceptually, the cold bridging effect should be similar at X-1 and X-2, however, the measured cold bridging effect is more prominent at X-2, which may be caused by test errors. For the temperatures in group X-3, the hot side temperature declines from location X-3-a to X-3-c, while the corresponding cold side temperature increases, which may be caused by the edge of the wall.

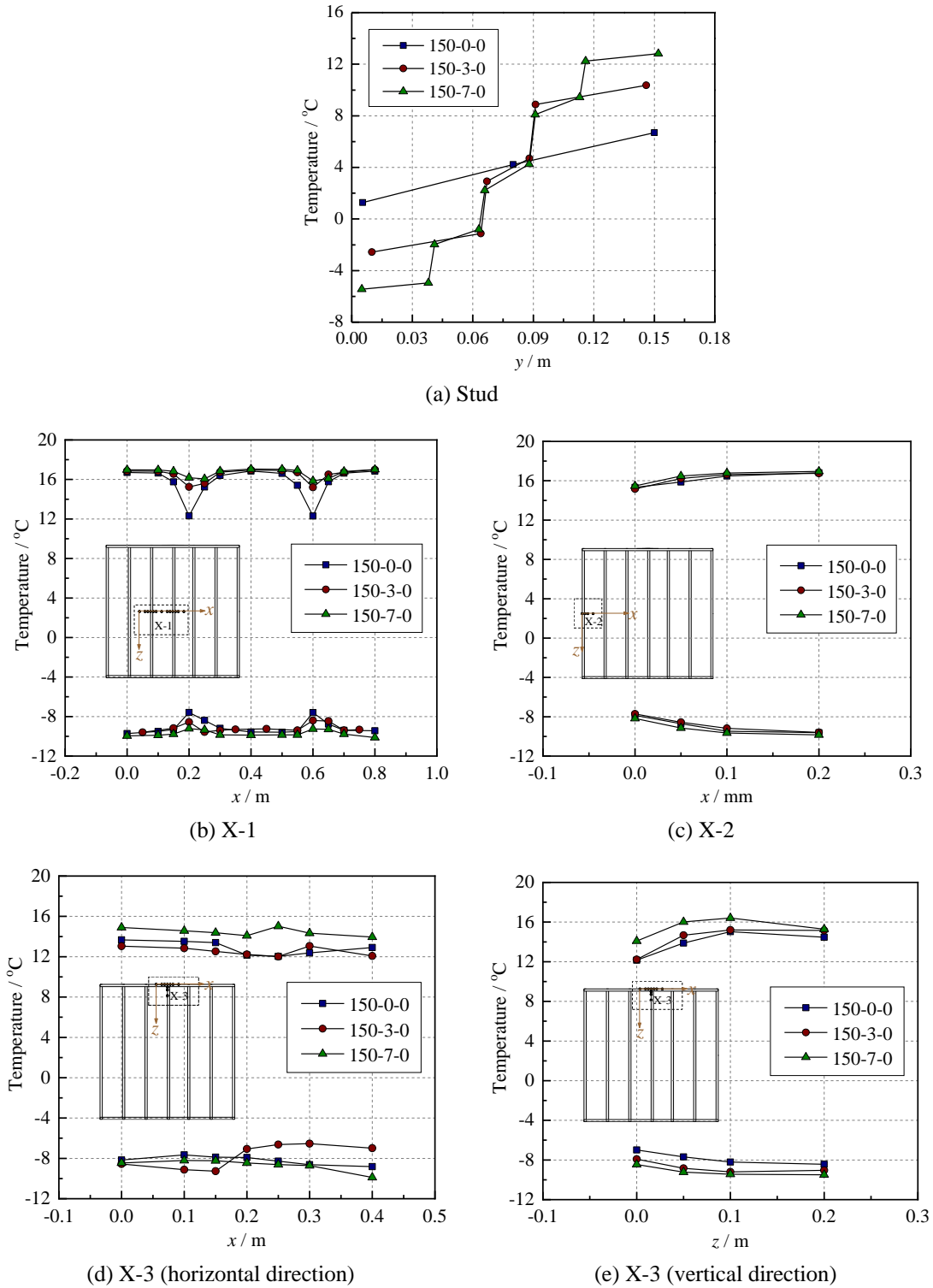


Fig. 6. Measured temperatures of specimens 150-0-0, 150-3-0 and 150-7-0.

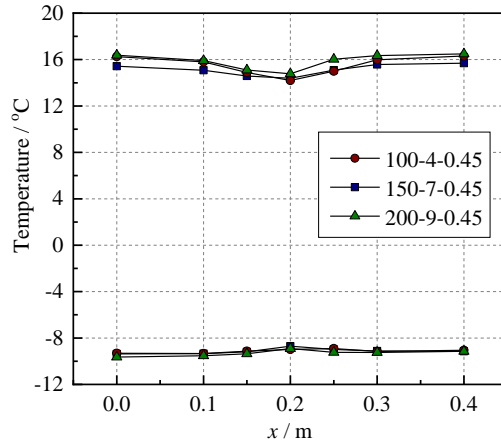


Fig. 7. Comparisons of temperatures of specimens 100-4-0.45, 150-7-0.45 and 200-9-0.45 (X-1).

Table 2. Test results of thermal transmittance of the wall

Specimen no.	150-0-0	150-3-0	150-7-0	150-7-0.45	100-4-0.45	200-9-0.45
Air temperature in hot box (°C)	17.80	17.76	17.78	17.78	17.75	17.76
Air temperature in cold box (°C)	-9.90	-9.92	-10.09	-9.86	-9.98	-9.94
Air temperature difference (°C)	27.70	27.68	27.87	27.64	27.63	27.70
Transferred heat (W)	86.7	69.7	61.17	52.3	74.03	42
Transferred heat via XPS (W)	--	--	--	13.84	19.19	10.84
Thermal transmittance of wall (W/(m ² K))	0.54	0.44	0.38	0.435	0.62	0.355
FE results (W/(m ² K))	0.59	0.464	0.356	0.42	0.578	0.325
Deviation (%)	8.5	5.2	-6.7	-3.6	-7.3	-8.3

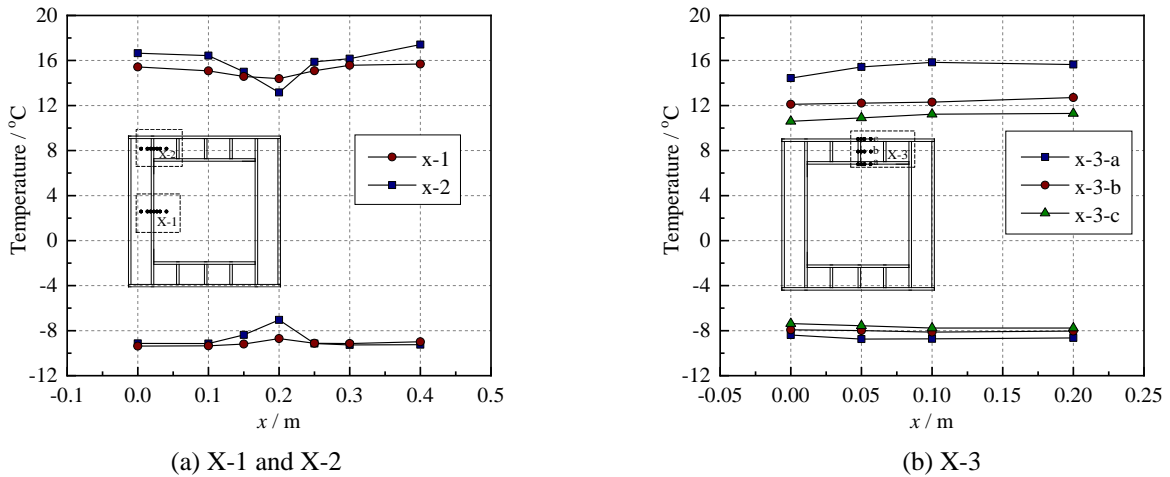


Fig. 8. Typical temperature comparisons (150-7-0.45).

The heat transfer coefficient can be obtained by calibrating the heat balance in the hot box. The measured thermal transmittances of these specimens are shown in Tab. 2. Thermal transmittance of these walls significantly decreases as the number of rows of perforations increases. Thermal transmittance decreases by 18.5% and 29.6% for specimens 150-3-0 and 150-7-0 in comparison with specimen 150-0-0. Thermal transmittance also decreases as wall thickness increases, which reaches 29.8% and 42.7% for specimens 150-7-0.45 and 200-9-0.45 in comparison with specimen 100-4-0.45. The wall with a window opening (specimen 150-7-0.45) has a greater thermal transmittance than the wall without an opening (specimen 150-7-0) because more steel studs were used in the wall with the opening.

3 Numerical analysis

3.1 Finite element numerical analysis model

A refined finite element (FE) model of the slotted steel stud wall was developed using ABAQUS software (Fig. 9). The thermal properties of materials, including mineral wool, gypsum plasterboard and steel were defined according to Chinese code GB50176-2016 [42], as shown in Tab. 3. The mineral wool and gypsum plasterboard were modelled using thermal analysis solid elements DC3D8, and steel studs were modelled using thermal analysis shell elements DS4. The heat transfer coefficient considering both convection and radiation was 8.7 W/(m² K) for the hot side of the wall and 23.0 W/(m² K) for the cold side [43]. All side surfaces were assumed to be adiabatic.

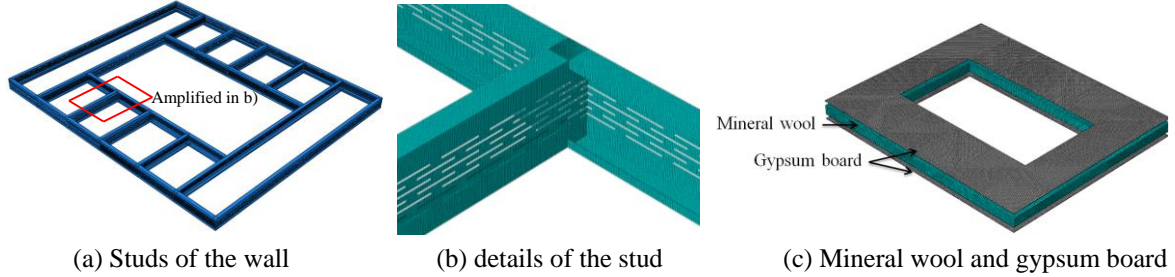


Fig. 9. Finite element model of the light gauge slotted steel stud wall.

Table 3. Thermophysical properties of materials [42]

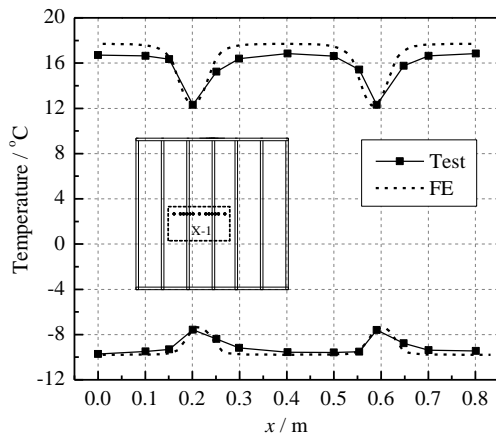
Material	Thermal conductivity (W/(m ² K))	Density (kg/m ³)	Specific heat (J/(kg K))
Steel stud	58.2	7850	480
Gypsum board	0.33	1050	1050
Mineral wool	0.05	70	840

3.2 Verification of the numerical model

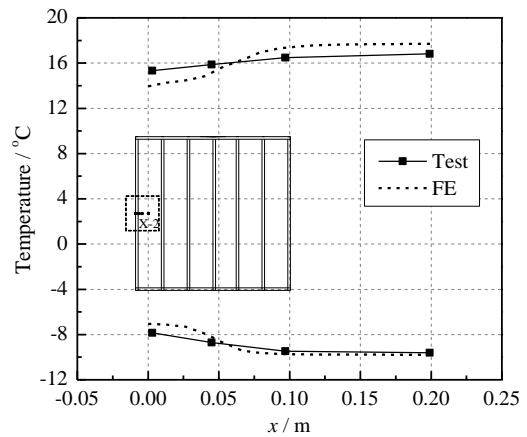
For simulations of these specimens, the thermal properties of mineral wool and gypsum board were defined according to test results, and measured air temperatures in the cold box and hot box were used (Tab. 4). The FE model results and the experimental results are shown in Figs. 10 - 11 for comparison. It can be seen that the FE model results agree well with the measured experimental temperatures. All experimental measurements and model temperature predictions are shown for comparison in Fig. 12, in which the standard deviation is within 5%. Similar results for thermal transmittance are shown in Fig. 13 and Tab. 2. Both sets of results confirm that there is good agreement between experimental results and model predictions.

Table 4. Measured air temperatures of cold box and hot box

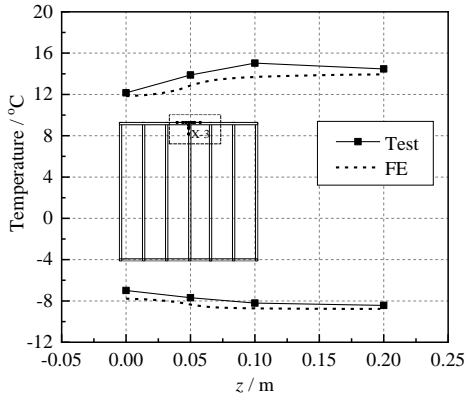
Specimen no.	150-0-0	150-3-0	150-7-0	150-7-0.45	100-4-0.45	200-9-0.45
Cold box (°C)	-9.92	-9.92	-10.09	-9.88	-9.86	-9.94
Hot box (°C)	17.78	17.76	17.78	17.75	17.78	17.76



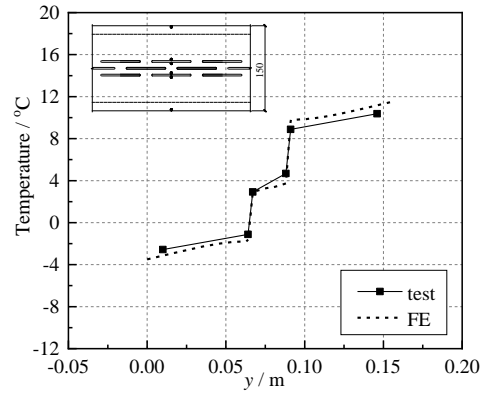
(a) 150-0-0 (X-1)



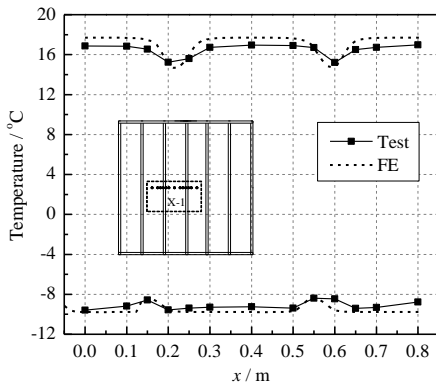
(b) 150-0-0 (X-2)



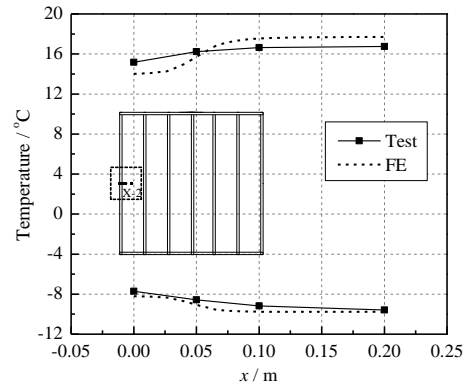
(c) 150-0-0 (X-3)



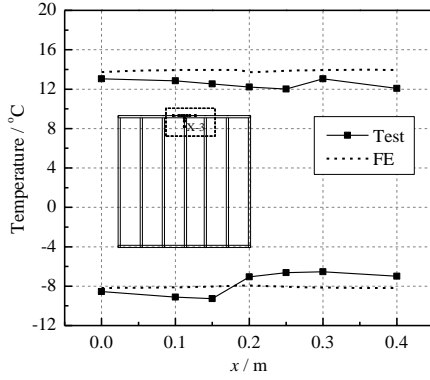
(d) 150-3-0 (stud)



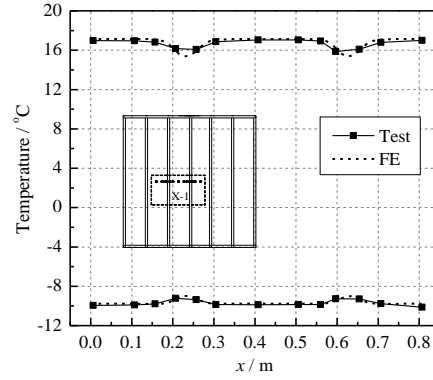
(e) 150-3-0 (X-1)



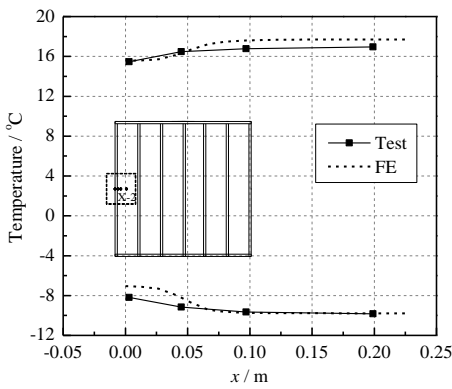
(f) 150-3-0 (X-2)



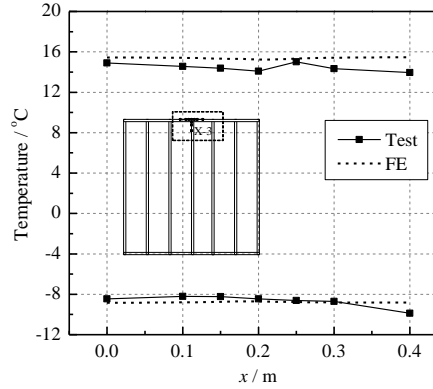
(g) 150-3-0 (X-3)



(h) 150-7-0 (X-1)



(i) 150-7-0 (X-2)



(j) 150-7-0 (X-3)

Fig. 10. Comparisons between FE and test temperatures of specimens 150-0-0, 150-3-0 and 150-7-0.

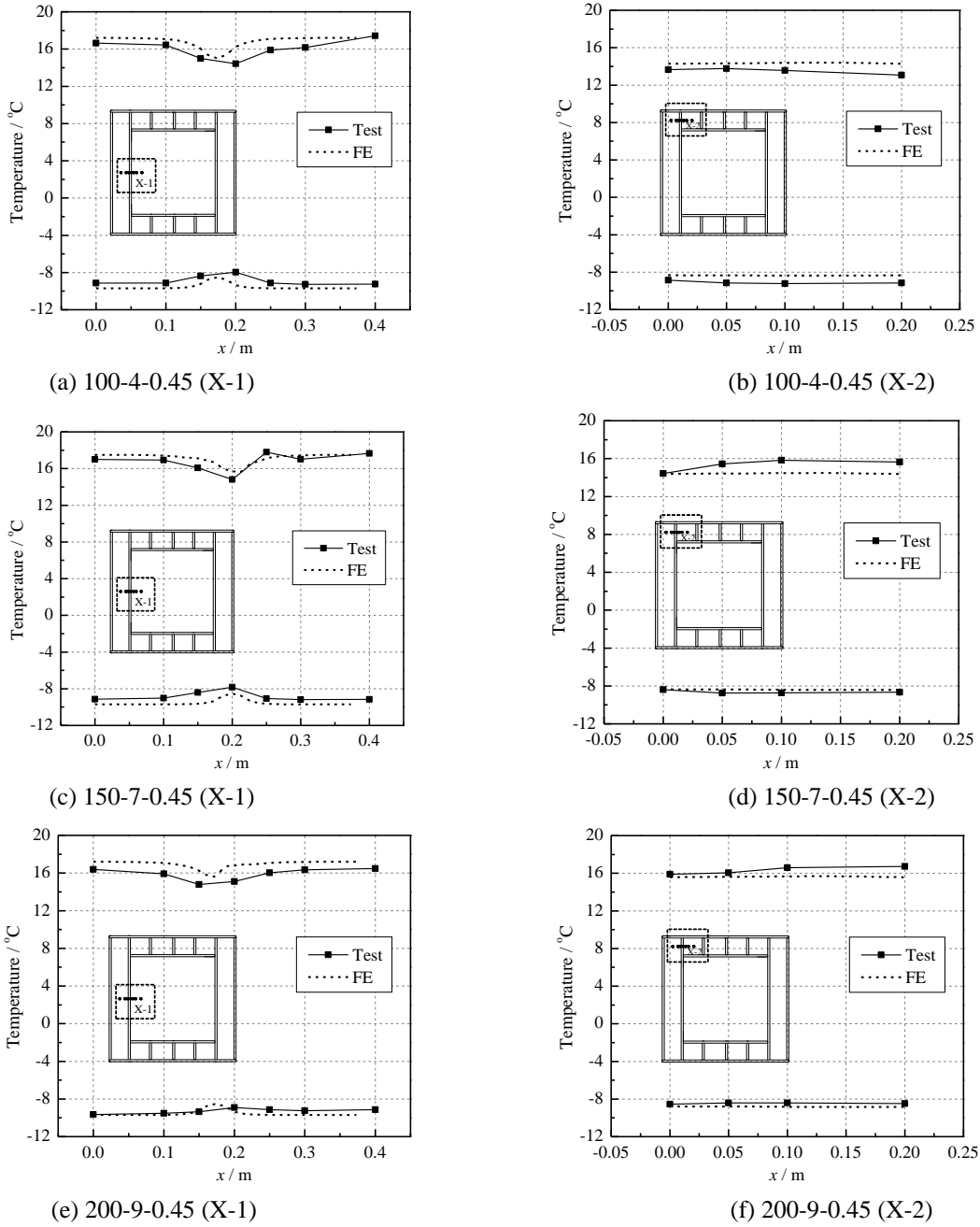


Fig. 11. Comparisons between FE and test temperatures of specimen 100-4-0.45, 150-7-0.45 and 200-9-0.45.

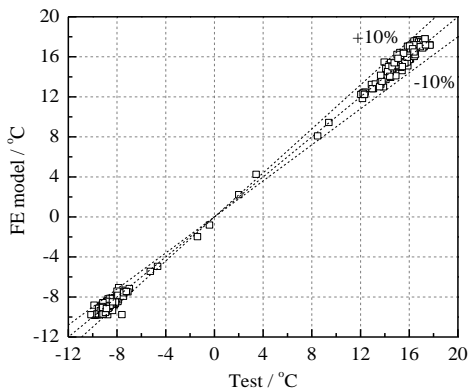


Fig. 12. Comparisons between experimental and FE model temperatures.

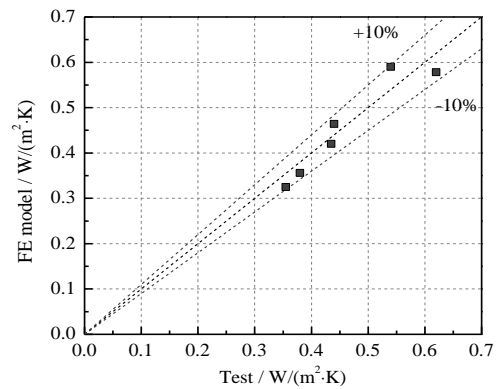


Fig. 13. Comparisons between experimental and FE model values of thermal transmittance.

3.3 Thermal bridging

A FE model of a single light gauge steel stud was developed to analyze thermal bridging. The web height of the stud was 200 mm, and there were zero or seven rows of perforations. Heat flux for the steel stud without perforations was uniform, but heat flux was rather irregular when there were perforations in the web, as shown in **Fig. 14**. Heat is transferred mainly by thermal conduction via the steel between perforations, and thus heat flux around perforations is greater than in other parts of the stud. The perforations greatly increase the path length of heat transfer, and the thermal resistance of the stud increases correspondingly.

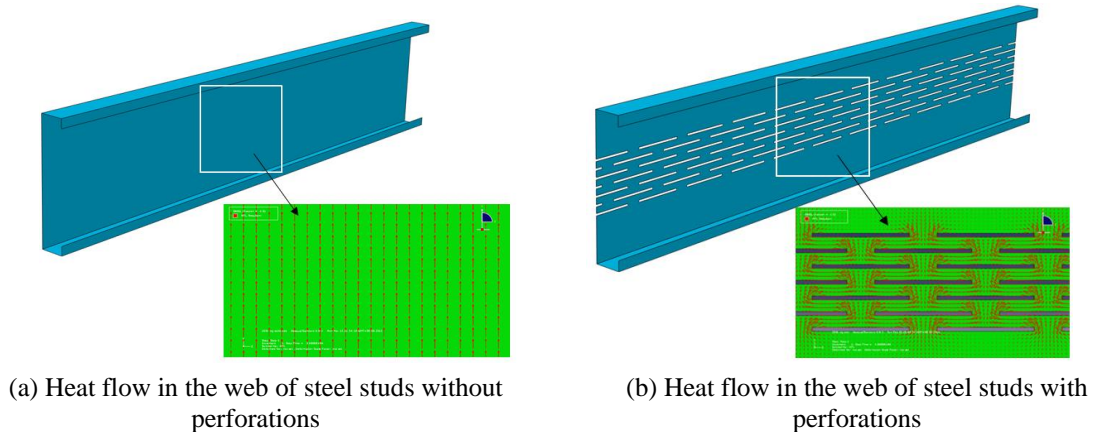


Fig. 14. Heat flow of light gauge steel stud with and without perforations.

A FE model of a light gauge slotted steel stud wall was also developed. The web height of the steel stud was 200 mm, gypsum board thickness was 12 mm, and mineral wool filler was incorporated as shown in **Fig. 1**. Seven rows of perforations were made in the web of the stud in this wall. Predicted temperatures for this wall are shown in **Fig. 15**, in which y is the position of points in the wall thickness direction. The cold side and hot side temperatures were set to be $-31\text{ }^{\circ}\text{C}$ and $18\text{ }^{\circ}\text{C}$ following Chinese code GB50176-2016, corresponding to the outdoor and indoor design temperatures of Harbin, a typical city in the severe cold region of China. For the wall fabricated with steel studs without perforations, the temperature of the studs is much lower than the temperature of the hot side of the mineral wool but much higher than the temperature of the cold side of the mineral wool. This clearly shows the effect of thermal bridging and can be explained by the thermal conductivity of the steel stud is greater than that of the mineral wool. When the stud web was perforated, the temperature changed abruptly at the position of the perforations, thus increasing the temperature gradient. Temperature differences between the hot sides and cold sides of steel studs without perforations, steel studs with perforations, and mineral wool were $22.5\text{ }^{\circ}\text{C}$, $34.6\text{ }^{\circ}\text{C}$ and $41.7\text{ }^{\circ}\text{C}$ respectively. The temperature difference between the hot side and cold side for the steel stud with seven rows of perforations was 53.8% greater than that for studs without perforations. This observation provides an evidence that thermal bridging can be reduced by incorporating perforations in the steel stud web.

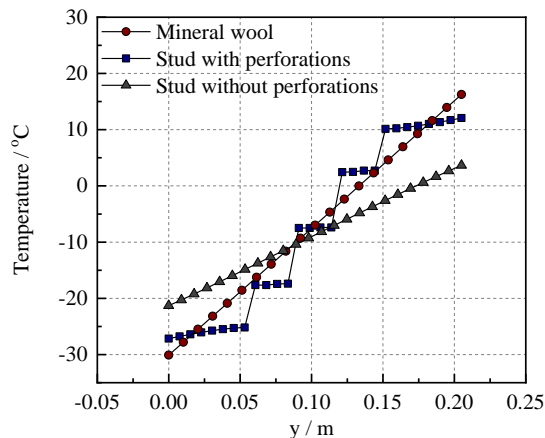


Fig. 15. Temperatures of steel stud and mineral wool.

3.4 Parametric studies

After validating the FE model, parametric studies were conducted to extend the ranges of key parameters (number of rows of perforations, web height, stud percentage, and thermal conductivity coefficients). **Fig. 16** (a) shows the relationship between thermal transmittance (U -value) and the number of rows of perforations. Thermal transmittance decreases as the number of rows of perforations increases, because the corresponding heat transfer path becomes longer. It can be found that the desired thermal transmittance can be achieved by placing perforations, which would be more economical than increasing wall thickness. For example, with a wall thickness of 100mm, when the web of the stud is configured with 4 rows of perforations, its thermal transmittance is equivalent to that of a wall with a thickness of 150mm without perforations in the stud's web. Compared to increasing the wall thickness to reduce the heat transfer coefficient, the method of perforating the stud's web reduces the consumption of wall materials and increases the usable indoor area, thus making perforation a more economical approach.

To better quantify the influence of perforations, the perforation ratio was defined as h/H , where h is the total height of the perforation zone and H is the web height (**Fig. 3**). A higher perforation ratio indicates more rows of perforations, and thus the thermal transmittance declines correspondingly (**Fig. 16** (b)). However, the efficiency becomes less with the increasing perforation ratio, as shown in **Fig. 16** (b). The thermal insulation is enhanced with the increasing rows of perforations, but the flexural capacity of the wall would decrease correspondingly. Therefore the maximum perforation ratio is recommended to be 0.5, taking into account both thermal insulation and flexural capacity.

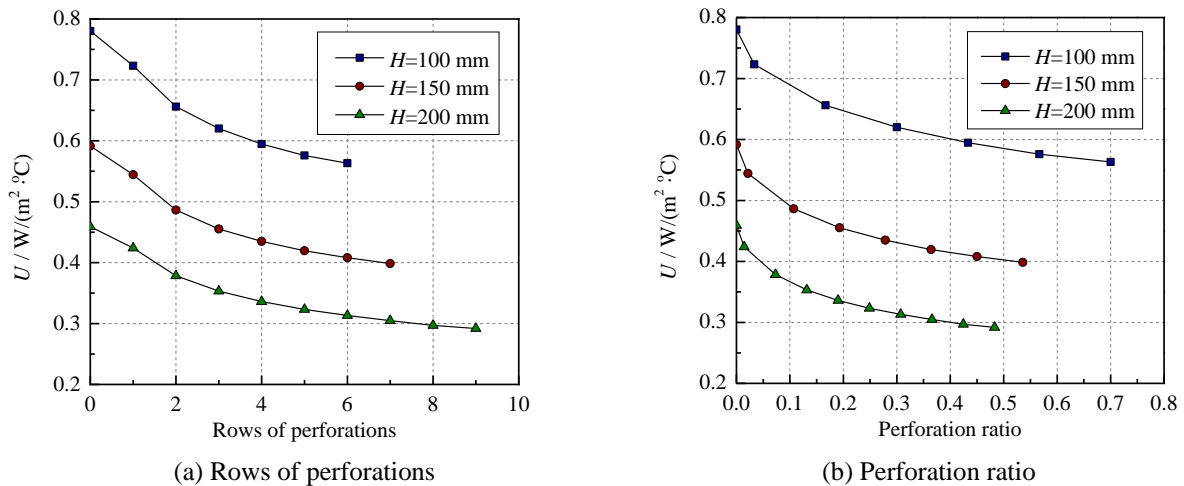


Fig. 16. Effect of the number of rows of perforations and perforation ratio on the thermal transmittance.

Fig. 17 shows the relationship between web height and thermal transmittance. An increase in web height increases the thickness of insulation materials and wall thickness. Thermal transmittance gradually reduces as web height increases, which means that the insulation gradually becomes more effective. When web height increases from 100 mm to 200 mm, thermal transmittance decreases by 43.6%. It can be seen that increasing web height significantly improves the performance of the insulation. However, the construction cost increases with the increase of web height, which may be explained by: i) the material consumption increases with the increasing web height, including both insulation material and steel stud, ii) the wall weight also increases and thus increasing the force transferred to the foundation, resulting in increased construction cost of the foundation. Therefore the wall thickness should be determined according to regional energy-saving design standards.

The relationship between thermal transmittance and the size of the window opening is not monotonic (**Fig. 18** (a)). The general stud spacing of the light gauge slotted steel stud wall was defined as 600 mm in the numerical simulation. However, extra studs may need to be placed around the window opening (e.g., **Fig. 2** (b)), which results in an abrupt change in thermal transmittance. Even for the same opening factor, the variation in window width and height has different influences on thermal transmittance, as shown in **Fig. 18** (a). Thus a key issue is how to quantify the influence of the opening factor. Thermal bridging in this kind of wall is concentrated at the steel stud flanges because of the high

thermal conductivity of steel. We devised the concept of stud percentage (defined as the ratio of the area of the stud flange to the wall area) to quantify the effect of the opening dimension on thermal transmittance. The relationship between thermal transmittance and stud percentage is shown in **Fig. 18** (b). Thermal transmittance increases significantly as the stud percentage increases: when the stud percentage increases from 0.14 to 0.24, thermal transmittance increases by 26.4%. Thus stud percentage should be strictly controlled during the design of this kind of wall. It should be noted that the thermal transmittance of walls in this study is calculated without considering the thermal conductivity of windows, which means that the window openings are assumed to be adiabatic. The window opening size was varied to identify the influence of steel studs around the opening (**Fig. 9** (a)). The linear thermal transmittance method can be used to calculate the thermal transmittance of walls with windows following the BC Standard [44,45]. A simpler method is specified in Chinese code JGJ 26-2010 [43], in which the thermal transmittance of the whole wall can be obtained by multiplying a factor greater than 1.0 to consider the effects of windows.

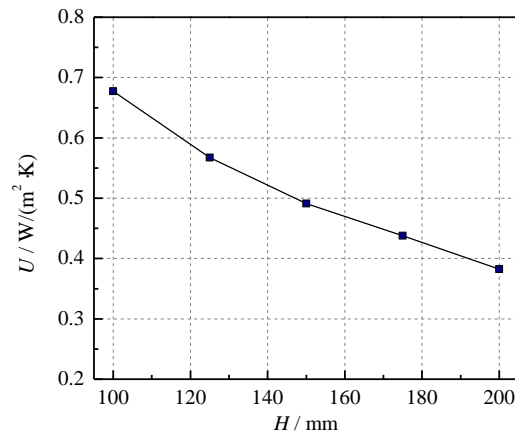


Fig. 17. Effect of web height on thermal transmittance of a wall.

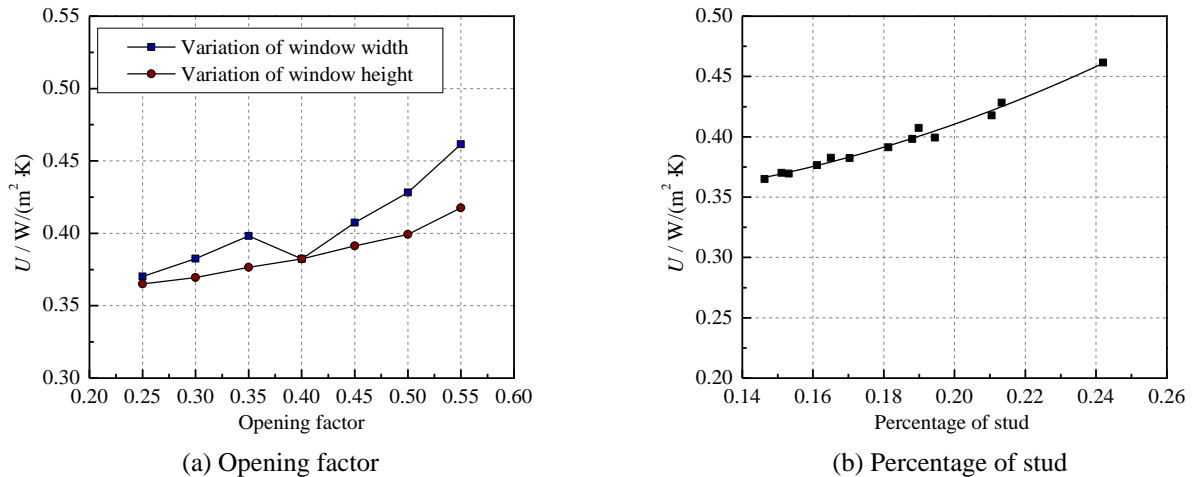


Fig. 18. Effect of opening factor and stud percentage on the thermal transmittance.

Properties of the construction materials (mineral wool, gypsum board) may also affect thermal transmittance in this kind of wall. **Fig. 19** (a) shows the relationship between the thermal transmittance of the wall and the thermal conductivity of the mineral wool insulation. As the main insulation material of the wall, the mineral wool's thermal conductivity has a significant influence on the thermal transmittance of the wall. The gypsum plasterboard is the first barrier to thermal bridging and blocks heat transfer. However, the thermal conductivity of the gypsum board has limited influence on the thermal transmittance of the wall (**Fig. 19** (b)), which may be explained by the relatively small thickness of the gypsum board compared with the thickness of the whole wall. In general, the thermal transmittance of the wall tends to increase linearly with the increased thermal conductivities of mineral wool and gypsum board.

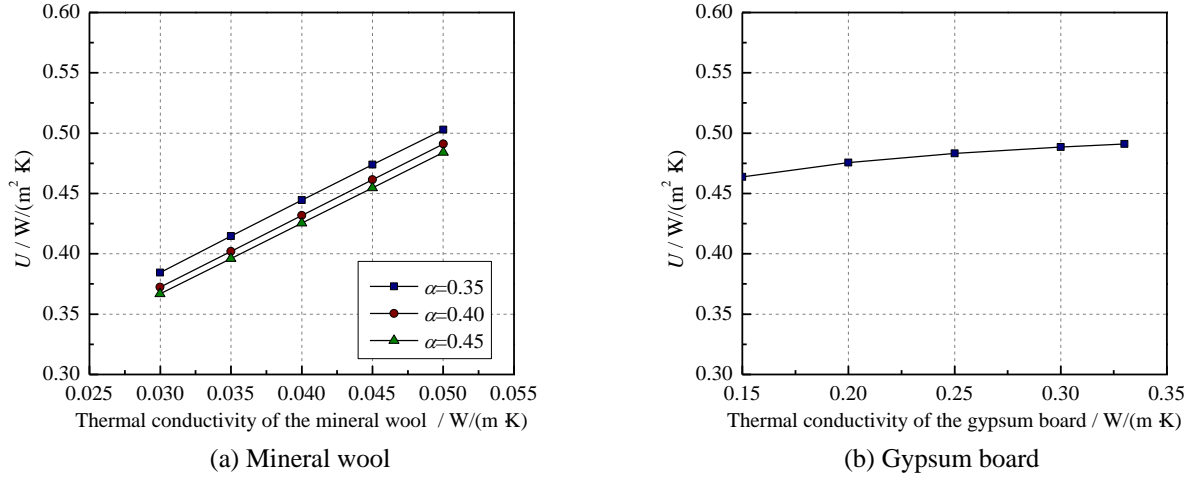


Fig. 19. Effect of thermal conductivities of materials on the thermal transmittance.

4 Design method

Tables for U-values or R-values [32,46] and simplified methods for calculating U-values and R-values [47,48] for light gauge steel stud walls that implicitly take account of thermal bridging have been developed in previous studies and codes. However, these tables are limited to specific wall thicknesses, specific numbers of rows of perforations, and specific window opening dimensions. Following the parallel path method specified in [48], we proposed a general method for calculating U-values for light gauge slotted steel stud walls that takes account of the effects of wall thickness, perforations, window openings, and the thermal properties of construction materials.

Thermal transmittance U of the wall can be predicted by:

$$U = \frac{1}{R} \quad (1)$$

where R is the thermal resistance of the wall.

If the wall consists of two or more homogeneous materials, the thermal resistance can be calculated from the thermal resistance of the different constituent materials:

$$R = \sum R_i = \sum \frac{D_i}{\lambda_i} \quad (2)$$

where R_i is the thermal resistance of the material at layer i , D_i is the thickness of the material at layer i , and λ_i is the thermal conductivity of the material at layer i .

The effects of perforations and multi-layered materials on thermal resistance cannot be directly calculated because of thermal bridging. Parametric studies show that web height, stud percentage and thermal conductivity are the main factors affecting the thermal insulation of this kind of wall. We devised a two-part equation that combined the thermal resistance of the insulation material with the thermal resistance of the sheathing board, consistent with the design method for light gauge steel frame walls specified in Thermal Design and Code Compliance for Cold-formed Steel Walls [48]. The thermal bridging of steel studs is accounted for by correcting the thermal resistance of the insulation material. The equation was proposed based on the FE model results of 216 walls, given as follows:

$$R = \frac{H}{\lambda_m/k} + \frac{H_g}{\lambda_g} \quad (3)$$

$$k = 0.9 - (0.16 + \gamma)(1.44 - \beta) \quad (4)$$

where H is the web height, λ_m is the thermal conductivity of the insulation material, k is a correction factor representing the effect of steel studs on thermal resistance, H_g is the thickness of the sheathing board, λ_g is the thermal conductivity of the sheathing board, γ is the stud percentage, and β is the perforation ratio.

Limits to the applicability of this method are: $H = 100 - 250$ mm, $\lambda_m = 0.03 - 0.05$ W/(m K), $\lambda_g = 0.15 - 0.33$ W/(m · K), $\gamma = 0.1 - 0.25$, $\beta = 0.2 - 0.6$, and rows of perforations ≥ 2 . The method applies to non-load-bearing light gauge slotted steel stud walls fabricated with C-runner profiles. Comparisons of results from the design method and the numerical simulation are shown in **Fig. 20** (a). The mean of the ratio of thermal transmittance predicted by the design method to that predicted by the FE model is 1.003 and the standard deviation is 0.037. These values confirm that the predictions of the design method agree well with the results of the FE model. Comparisons of the predicted results of the design method and the experimental results are shown in **Fig. 20** (b). The mean of the ratio of thermal transmittance predicted by the design method to that observed in experiments is 0.964 and the standard deviation is 0.074. The proposed equation (which takes account of wall thickness, web perforations, window openings, and thermal properties of construction materials) has high prediction accuracy and a clear physical meaning.

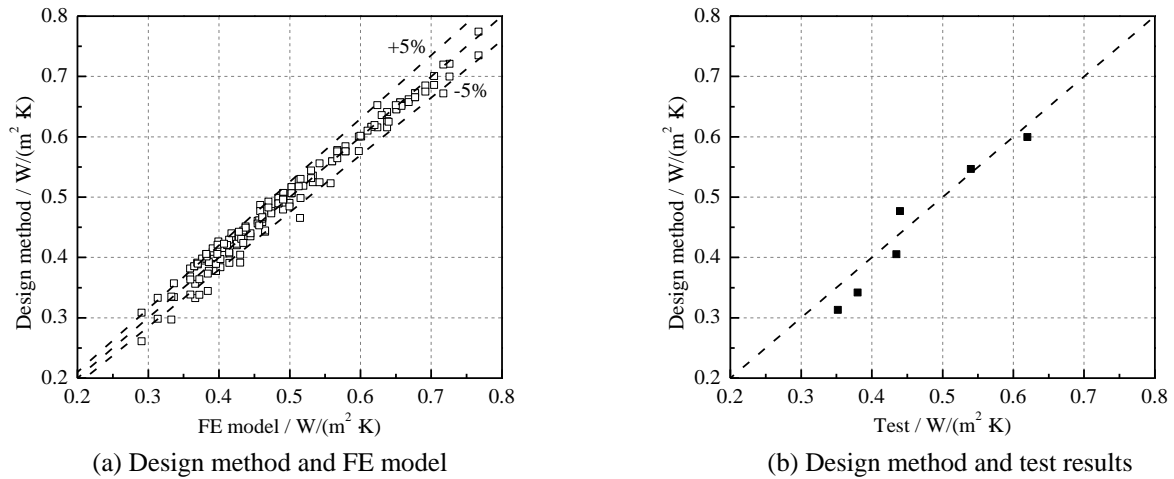


Fig. 20. Comparisons of predicted thermal transmittance.

5 Conclusions

Experiments on six non-load-bearing light gauge slotted steel stud wall specimens were conducted using a hot box, in which the number of rows of perforations, stud web height, and the ratio of window area to wall area were considered. Temperatures of the steel studs and gypsum plasterboard were measured and thermal transmittances were obtained. Then a finite element model was developed using ABAQUS software to further investigate the thermal performance of this kind of wall. The following conclusions can be drawn from this work:

(1) The thermal transmittance declines significantly as the increases in web height and the number of rows of perforations. The thermal transmittance reduces by 25.0%-36.8% for the wall with a stud web height of 100 mm -200 mm and a perforation ratio of 0.5, while the thermal transmittance reduces by 43.6% when the stud web height increases from 100 mm to 200 mm. Compared with increasing web height (wall thickness), placing perforations in stud webs is a more economical method to improve the insulation of the wall.

(2) An opening in the wall (such as a window) has a significant effect on thermal insulation because additional steel studs would be placed around window openings. However, it is difficult to precisely quantify the relationship between opening and thermal transmittance because the size of the opening affects the stud configuration. A concept of stud percentage was proposed to quantify the effect of an opening on the thermal transmittance of this kind of wall and its feasibility was verified. The stud percentage increases from 14.6% to 24.2% leading to a 26.4% increase in thermal transmittance for the typical wall with a stud height of 100 mm.

(3) A general design method was proposed for calculating the thermal transmittance of non-load-bearing light gauge slotted steel stud walls, considering the influences of web height, stud perforations, window opening dimensions, and thermal conductivities of fabricated materials.

Funding Statement

The author(s) received no specific funding for this study.

CRedit authorship contribution statement

Yuyin Wang: Conceptualization, Supervision. **Faqi Liu:** Investigation, Formal analysis, Writing – original draft. **Hua Yang:** Conceptualization, Writing – review & editing. **Feng Fu:** Writing – review & editing. **Yuteng Yan:** Investigation, Validation, Data Curation.

Conflicts of Interest

The authors declare that they have no conflicts of interest to report regarding the present study.

References

- [1] Veljkovic M, Johansson B. Light steel framing for residential buildings. *Thin-walled structures* 2006; 44(12): 1272-1279. <https://doi.org/10.1016/j.tws.2007.01.006>.
- [2] Miller T H, Pekoz T. Behavior of cold-formed steel wall stud assemblies. *Journal of structural Engineering* 1993; 119(2): 641-651. [https://doi.org/10.1061/\(ASCE\)0733-9445\(1993\)119:2\(641\)](https://doi.org/10.1061/(ASCE)0733-9445(1993)119:2(641)).
- [3] Tian Y S, Wang J, Lu T J, et al. An experimental study on the axial behaviour of cold-formed steel wall studs and panels. *Thin-walled structures* 2004; 42(4): 557-573. <https://doi.org/10.1016/j.tws.2003.09.004>.
- [4] Salhab B, Wang Y C. Equivalent thickness of cold-formed thin-walled channel sections with perforated webs under compression. *Thin-Walled Structures* 2008; 46(7-9): 823-838. <https://doi.org/10.1016/j.tws.2008.01.029>.
- [5] Wang Y C, Salhab B. Structural behaviour and design of lightweight structural panels using perforated cold-formed thin-walled sections under compression. *International Journal of Steel Structures* 2009; 9(1): 57-67. <https://doi.org/10.1007/bf03249480>.
- [6] Vieira Jr L C M, Shifferaw Y, Schafer B W. Experiments on sheathed cold-formed steel studs in compression. *Journal of Constructional Steel Research* 2011; 67(10): 1554-1566. <https://doi.org/10.1016/j.jcsr.2011.03.029>.
- [7] Ye J, Feng R, Chen W, et al. Behavior of cold-formed steel wall stud with sheathing subjected to compression. *Journal of Constructional Steel Research* 2016; 116: 79-91. <https://doi.org/10.1016/j.jcsr.2015.08.028>.
- [8] Sonkar C, Mittal AK, Bhattacharyya SKr. Comparative study on cold-formed steel single-stud and multiple-studs wall panels with magnesium oxide sheathing under axial loading: experimental and analytical. *Journal of Structural Engineering* 2020; 146:04020224. [https://doi.org/10.1061/\(ASCE\)ST.1943-541X.0002723](https://doi.org/10.1061/(ASCE)ST.1943-541X.0002723).
- [9] Liu C, Mao X, He L, et al. A new demountable light-gauge steel framed wall: Flexural behavior, thermal performance and life cycle assessment. *Journal of Building Engineering*, 2022; 47: 103856. <https://doi.org/10.1016/j.job.2021.103856>
- [10] Degtyareva N, Gatheeshgar P, Poologanathan K, et al. Local buckling strength and design of cold-formed steel beams with slotted perforations. *Thin-Walled Structures*, 2020; 156: 106951. <https://doi.org/10.1016/j.tws.2020.106951>.
- [11] Chang Y, Wang Y, Lin J, et al. Experimental study on flexural behaviors of slotted light-gauge steel stud walls subjected to distributed loading. *Journal of Building Structures*, 2023; 44(4): 297. <https://doi.org/10.14006/j.jzjgxb.2022.C030> (in Chinese)
- [12] Perera D, Poologanathan K, Gatheeshgar P, et al. Fire performance of modular wall panels: Numerical analysis. *Structures*, 2021; 34: 1048-1067. <https://doi.org/10.1016/j.istruc.2021.06.111>.
- [13] Alfawakhiri F, Sultan M A, MacKinnon D H. Fire resistance of loadbearing steel-stud wall protected with gypsum board: a review. *Fire Technology* 1999; 35(4): 308-335. <https://doi.org/10.1023/A:1015401029995>.
- [14] Feng M, Wang Y C, Davies J M. Thermal performance of cold-formed thin-walled steel panel systems in fire. *Fire safety journal* 2003; 38(4): 365-394. [https://doi.org/10.1016/S0379-7112\(02\)00090-5](https://doi.org/10.1016/S0379-7112(02)00090-5).
- [15] Feng M, Wang Y C. An analysis of the structural behaviour of axially loaded full-scale cold-formed thin-walled steel structural panels tested under fire conditions. *Thin-walled structures* 2005; 43(2): 291-332. <https://doi.org/10.1016/j.tws.2004.07.008>.
- [16] Kodur V K R, Sultan M A. Factors influencing fire resistance of load-bearing steel stud walls. *Fire technology* 2006; 42(1): 5-26. <https://doi.org/10.1007/s10694-005-3730-y>.
- [17] Chen W, Ye J, Bai Y, Zhao X L. Full-scale fire experiments on load-bearing cold-formed steel walls lined with different panels. *Journal of Constructional Steel Research* 2012; 79: 242-254. <https://doi.org/10.1016/j.jcsr.2012.07.031>.
- [18] Shahbazian A, Wang Y C. A simplified approach for calculating temperatures in axially loaded cold-formed thin-walled steel studs in wall panel assemblies exposed to fire from one side. *Thin-Walled Structures* 2013;

- 64: 60-72. <https://doi.org/10.1016/j.tws.2012.12.005>.
- [19] Ariyanayagam A D, Mahendran M. Fire design rules for load bearing cold-formed steel frame walls exposed to realistic design fire curves. *Fire Safety Journal* 2015; 77: 1-20. <https://doi.org/10.1016/j.firesaf.2015.05.007>.
- [20] Ariyanayagam A D, Mahendran M. Fire tests of non-load bearing light gauge steel frame walls lined with calcium silicate boards and gypsum plasterboards. *Thin-Walled Structures* 2017; 115: 86-99. <https://doi.org/10.1016/j.tws.2017.02.005>.
- [21] Liu F, Fu F, Wang Y, et al. Fire performance of non-load-bearing light-gauge slotted steel stud walls. *Journal of Constructional Steel Research* 2017; 137: 228-241. <https://doi.org/10.1016/j.jcsr.2017.06.034>.
- [22] Ariyanayagam A D, Mahendran M. Residual capacity of fire exposed light gauge steel frame walls. *Thin-Walled Structures* 2018; 124: 107-120. <https://doi.org/10.1016/j.tws.2017.11.048>.
- [23] Gnanachelvam S, Ariyanayagam A, Mahendran M. Fire resistance of light gauge steel framed wall systems lined with PCM-plasterboards. *Fire Safety Journal* 2019; 108: 102838. <https://doi.org/10.1016/j.firesaf.2019.102838>.
- [24] Magarabooshan H, Ariyanayagam A, Mahendran M. Fire resistance of non-load bearing LSF walls with varying cavity depth. *Thin-Walled Structures* 2020; 150: 106675. <https://doi.org/10.1016/j.tws.2020.106675>.
- [25] Gong C, Sun D, Chen Q, et al. Seismic Performance of Modular Structures with Novel Steel Frame: Light Gauge Slotted Steel Stud Walls. *Shock and Vibration*, 2022, 2022: 6926657. <https://doi.org/10.1155/2022/6926657>
- [26] Fülöp L A, Dubina D. Performance of wall-stud cold-formed shear panels under monotonic and cyclic loading: Part I: Experimental research. *Thin-Walled Structures* 2004; 42(2): 321-338. [https://doi.org/10.1016/S0263-8231\(03\)00063-6](https://doi.org/10.1016/S0263-8231(03)00063-6).
- [27] Dubina D. Behavior and performance of cold-formed steel-framed houses under seismic action. *Journal of Constructional Steel Research* 2008; 64(7-8): 896-913. <https://doi.org/10.1016/j.jcsr.2008.01.029>.
- [28] Gao W C, Xiao Y. Seismic behavior of cold-formed steel frame shear walls sheathed with ply-bamboo panels. *Journal of Constructional Steel Research* 2017; 132: 217-229. <https://doi.org/10.1016/j.jcsr.2017.01.020>.
- [29] Höglund T, Burstrand H. Slotted steel studs to reduce thermal bridges in insulated walls. *Thin-Walled Structures* 1998; 32(1): 81-109. [https://doi.org/10.1016/S0263-8231\(98\)00028-7](https://doi.org/10.1016/S0263-8231(98)00028-7).
- [30] Salomvaara M, Nieminen J. Hygrothermal performance of a new light gauge steel-framed envelope system. *Journal of Thermal Envelope and Building Science* 1998; 22(2): 169-182. <https://doi.org/10.1016/B978-008043014-0/50184-0>.
- [31] Elhadj N R. Development of cost-effective, energy-efficient steel framing. Final Report, AISI/DOE Technology Roadmap Program, Pittsburgh, PA, USA, 2003. <https://scholarsmine.mst.edu/ccfss-aisi-spec/108>.
- [32] Lipták-Váradi J. Equivalent thermal conductivity of steel girders with slotted web. *Periodica Polytechnica. Civil Engineering* 2010; 54(2): <https://doi.org/10.3311/pp.ci.2010-2.12>.
- [33] Moore T V, Cruickshank C A, Beausoleil-Morrison I, et al. Thermal evaluation of a highly insulated steel stud wall with vacuum insulation panels using a guarded hot box apparatus. *Journal of Building Physics* 2021; 45(3): 303-322. <https://doi.org/10.1177/1744259120980030>.
- [34] Martins C, Santos P, da Silva L S. Lightweight steel-framed thermal bridges mitigation strategies: A parametric study. *Journal of Building Physics* 2016; 39(4): 342-372. <https://doi.org/10.1177/1744259115572130>.
- [35] Yang Z, Sun L, Nan B, et al. Thermal Performance of Slotted Light Steel-Framed Composite Wall. *Energies*, 2023, 16(5): 2482. <https://doi.org/10.3390/en16052482>
- [36] American Society of Heating, Refrigerating and Air Conditioning Engineers, Inc. ASHRAE handbook of fundamentals. ASHRAE Handbook of Fundamentals, 2017.
- [37] European Commission, Directorate-General for Research and Innovation, Strömber, J., Kergen, R., Lawson, M., Development of dry composite construction systems based on steel in residential applications: final report, Publications Office, 2002.
- [38] Kosny J, Christian J E. Thermal evaluation of several configurations of insulation and structural materials for some metal stud walls. *Energy and buildings* 1995; 22(2): 157-163. [https://doi.org/10.1016/0378-7788\(94\)00913-5](https://doi.org/10.1016/0378-7788(94)00913-5).
- [39] ISO E N. 8302. Thermal insulation-determination of steady-state thermal resistance and related properties-guarded hot plate apparatus. International Standards Organization, Geneva, 1991.
- [40] ISO standard 8990. Thermal insulation-determination of steady-state thermal resistance and related properties-calibrated and guarded hot box. International Standards Organization, Geneva, 1994.
- [41] GB/T 5480-2008. Test methods for mineral wool and its products. Standardization Administration of the People's Republic of China, 2008 (in Chinese).
- [42] GB 50176-2016. Code for Thermal Design of Civil Engineering. Ministry of Housing and Urban-Rural Development of the People's Republic of China (MOHURD), 2016 (in Chinese).

- [43] JGJ 26-2010. Design Standard for Energy Efficiency of Residential Buildings in Severe Cold and Cold Zones. Ministry of Housing and Urban-Rural Development of the People's Republic of China (MOHURD), 2010 (in Chinese).
- [44] Hershfield, M. 2011. Thermal performance of building envelope details for mid- and high-rise buildings. Final Report, ASHRAE Research Project RP-1365.
- [45] Hershfield M. Building Envelope Thermal Bridging Guide, version 1.6. Vancouver, BC: Hydro Power Smart, 2016.
- [46] CSSBI. Lightweight steel framing - architectural design guide. Canadian Sheet Steel Building Institute, 2002.
- [47] Gorgolewski M. Developing a simplified method of calculating U-values in light steel framing. Building and Environment 2007; 42(1): 230-236. <https://doi.org/10.1016/j.buildenv.2006.07.001>.
- [48] Steel Framing Alliance. Thermal Design and code compliance for cold-formed steel walls. American Iron and Steel Institute, 2015.